Springer

KSME

Journal of Mechanical Science and Technology 29 (10) (2015) 4167~4178
www.springerlink.com/content/1738-494x(Print)/1976-3824(Online)
DOI 10.1007/s12206-015-0911-6

Investigating the possibility of replacing IN 738LC gas turbine blades with IN 718 †

Farid Vakili-Tahami and Mohammad Reza Adibeig*

Department of Mechanical Engineering, University of Tabriz, Tabriz, Iran

(Manuscript Received November 2, 2014; Revised March 1, 2015; Accepted May 18, 2015)

Abstract

The possibility of replacing IN 738LC gas turbine blades with IN 718 is investigated in terms of their creep behavior at different working conditions. The latter superalloy is domestically produced and therefore there is a strong interest in using this alloy in manufacturing gas turbine blades. For this purpose, first the creep behavior and constitutive equation of IN 718 have been determined using experimental data. Test samples were machined from as-received bars and their physical and mechanical properties together with their creep behavior were examined. Constant load uni-axial creep tests were carried out at two constant temperatures of 660 and 675°C. Initial stresses range from 490 to 690 MPa that are below the yield stress at each temperature level. The test results verify the quality of the domestically produced superalloy and show that its characteristics match with the international standards. In addition, numerical optimization techniques were used to obtain creep constitutive parameters of the produced alloy based on the experimental data. Then, the creep behavior of gas turbine blades, which operate at different rotating speeds, was investigated using finite element method. The results show that since the creep deformation of IN 718 is high, it can only be used in low and medium power gas turbines.

Keywords: Creep constitutive equation; Superalloy; IN 718; IN 738LC; Gas turbine blade

1. Introduction

In the design of components operating at elevated temperatures, creep behavior should be considered primarily. Creep is the time-dependent deformation of a material under constant stress leading to a permanent change in shape and it is accelerated by increasing stress or temperature level. Creep fracture is normally related to the tertiary creep and is characterized mainly by the nucleation, growth, and coalescence of microscopic internal cavities [1, 2]. Creep behavior of materials is usually divided into primary, secondary and tertiary stages. In the primary stage, the creep rate is high at first, but it soon decreases. Secondary or steady state creep follows this stage, when the creep rate is low and almost constant. In third stage, creep rate increases rapidly and it results in creep fracture. Most engineering parts operate in the secondary stage or in a condition that failure occurs before creep fracture. In terms of creep behavior, this failure is usually regarded as excessive deformation [3, 4]. Hence, most creep analysis is based on constitutive equations, which model secondary creep [4].

Over the past decades, considerable efforts have been made to gain a fundamental understanding of creep behavior of mechanical components. Also, new alloys, such as Inconels (IN), Waspaloys and Hastelloys have been introduced with excellent ability to operate at high temperatures under multi-axial stress states. Creep testing procedures according to the operating conditions require expensive and often unachievable long-time tests. Thus, tests usually have been carried out at uni-axial condition at high temperature and stress levels [3]. For example, creep strain and creep life predictions for IN 718 were carried out by Yeom and Kim et al. [1] and constitutive equations for this superalloy determined by using omega method. In addition, Kim et al. [2] determined stress rupture characteristics of IN 718 alloy used in ramjet combustor. The steady state creep deformation of IN 718 was investigated by Han and Chaturvedi [4]. High temperature deformation of IN 718 was investigated by Thomas et al. [5]. Chen and Chaturvedi [6] investigated the effect of grain precipitates on the creep behavior of IN 718. They observed that the presence of precipitates at grain boundaries increases the creep rate and the stress exponent of the creep constitutive equation. Ankit and Prasad [7] simulated the creep cavity growth in IN 718 and studied the influence of surface and grain boundary diffusion.

In this paper, the creep behavior of domestically produced IN 718 superalloy has been investigated based on uni-axial creep tests to ensure that the quality of the product is acceptable. In addition, using the experimental data, the creep constitutive parameters have been obtained, which can be used to model the creep behavior of mechanical engineering parts made of this superalloy operating at different conditions.

*Corresponding author. Tel.: +98 4133392463, Fax.: +98 4133354153
E-mail address: mr.adibeig@tabrizu.ac.ir
† Recommended by Associate Editor Ki-Hoon Shin

Table 1. Chemical compositions of Inconel 718 (% Weight).

Element	Sample composition (%)	Standard composition (%) [2]
Ni	53	55.0-55.5
Cr	18.2	17.0-21.0
Fe	18.1	18.5
Mo	2.8	3.0
Ti	1.1	0.65-1.15
Co	0.98	1.00
Nb+Ta	5.2	5.1

Based on the developed constitutive equations, the creep behavior of a gas turbine blade, which is produced using this alloy, has been investigated. For this purpose, a finite element model has been developed and using numerical solutions, temperature, stress and strain distributions on the blade have been obtained to compare its creep behavior with the same blade manufactured of IN 738LC. The results of these comparisons clarify the possibility of using IN 718 in producing gas turbine blades.

2. Characteristics of the material

The material tested in this study was IN 718 nickel based superalloy. This type of superalloy was introduced in the 1940's. The early products contained 80% Ni and 20% Cr. Since then, other alloying elements such as titanium, aluminum, and tungsten have been added to enhance their thermo-mechanical properties [8]. IN 718 contains a large amount of Ni. Like all nickel based superalloys, it is precipitation hardened and contains both coherent γ' and γ" particles, whereas the major strengthening precipitate is the latter [8]. In this superalloy, Ni and Cr crystallize as a face-centered cubic phase γ. Also, Ti and Al precipitate in the form of intermetallic cubic crystal known as γ'. Nb can also form hardening precipitates of γ" which is a metastable inter-metallic compound Ni3Nb, which is a centered tetragonal crystal [6]. The existence of γ" particles sets the operating temperature limit of the material to about 650°C.

IN 718 can be hardened by aging and often involves joining by fusion welding [9]. It has wide application in power generating and aero-space industry [10, 11] due to its superior mechanical properties, acceptable weldability, resistance to strain-aged cracking during post-weld heat treatment and excellent resistance to oxidation at elevated temperatures [9, 12, 13].

The chemical composition of the as-received domestically produced sample is given in Table 1, along with the standard compositions for IN 718. It can be seen that the value of Ni, Mo and Co components for the domestically produced alloy are slightly less than the standard values. Ni and Cr increase the corrosion and oxidation resistance of the superalloy at high temperature. In addition, Co provides extra mechanical and corrosion resistance. Therefore, it is expected that the mechanical and creep behavior of the sample is different from the standard levels. These differences are major reasons that initiated this research program to investigate the mechanical and creep behavior of this alloy.

Table 2. Results of tension test on Inconel 718 at room temperature.

Tension test	E-modulus (kN/mm^2)	Rp 0.2 (N/mm^2)	Max stress (N/mm^2)	ε break%
As-received	286.97	475.53	873.88	40.45
Aged hardened	209.69	1110.77	1335.70	18.60
Standard [2]	209	1227	1423	15.54

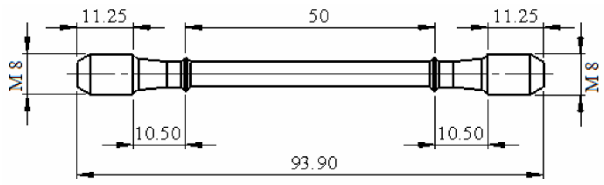

Fig. 1. Uni-axial creep test specimen according to the ASTM E8M-04 [14] with gauge length of 50 mm and diameter of 5 mm. Dimensions are in mm.

3. Experimental tests

To study the creep properties of the material, test samples were cut from as-received bars using wire-cutting method and then machined to conform to ASTM A276-05a specifications and ASTM E8M-04 [14]. Gauge length of the samples is 50 mm with the diameter of 5 mm (see Fig. 1). The uni-axial creep tests have been carried out under constant initial stresses of 565, 610 and 690 MPa at 660°C; and 490, 545 and 565 MPa at 675°C. During the tests, the temperature and load levels remain constant. The excellent creep and anti-oxidation properties of IN 718 prevail at temperatures as high as 650°C [15]; therefore, to investigate the hot-work ability of the domestically produced alloy, all tests were above this temperature level. In standard creep tests, the stress levels should be far below the yield stress of the alloy at the test-temperatures to prevent initial plasticity. Therefore, all the stress levels during the tests were selected to be lower than the yield stress with a factor of about 1.5. The exact stress level depends on the limitations imposed by the testing machine and the exact cross section of the sample.

3.1 Tension tests

At the first stage, the tensile properties of the as-received material and the effect of heat treatment on its mechanical characteristics have been investigated. To obtain the best combination of the tensile and stress rupture properties, the following heat treatment was used: 1hr at 954 to 982°C then air cooled + 8hrs at 718°C then cooling with the rate of 55°C/hr to 621°C, held for 8hrs and air cooled [6]. In Table 2,

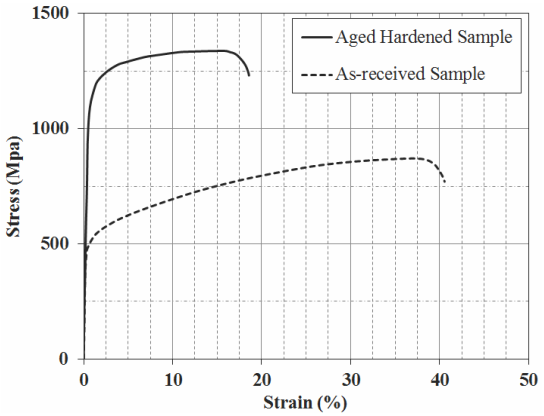

Fig. 2. Stress-strain curves for as-received and aged hardened samples.

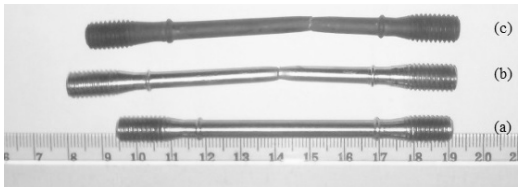

Fig. 3. Differences of elongation in tension test: (a) fabricated sample; (b) as-received; (c) aged hardened.

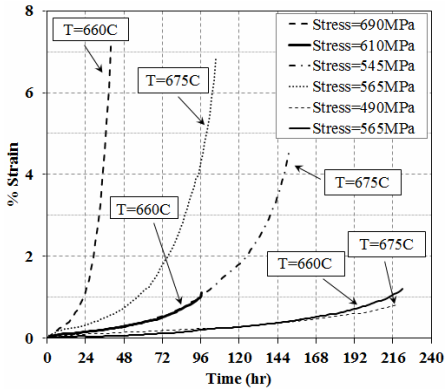

Fig. 4. Creep strain-time curves for aged hardened IN 718.

the results of tension tests at room temperature are shown. The aged hardened samples have better mechanical strength than as-received samples and their results are close to the results in standard catalogs. The stress-strain curves of aged hardened and as-received samples are depicted in Fig. 2.

In Fig. 3, the differences in the elongation of tested samples are shown. Because of the lower tensile resistance, as-received samples have higher elongation than aged hardened ones.

The results show that the superior characteristics of IN 718 prevail after aged hardening and therefore it is usually used in this condition.

3.2. Creep tests

All the creep tests were on aged hardened samples. In Fig. 4,

Table 3. Uni-axial creep testing results for the Inconel 718.

Temperature	Stress (MPa)	Rupture time (hr)	Min. creep strain rate (1/hr)
660	565	222	2.21E-3
660	610	96	4.90E-3
660	690	40	3.18E-2
675	490	223.5	2.10E-3
675	545	151	5.10E-3
675	565	105.5	1.10E-2

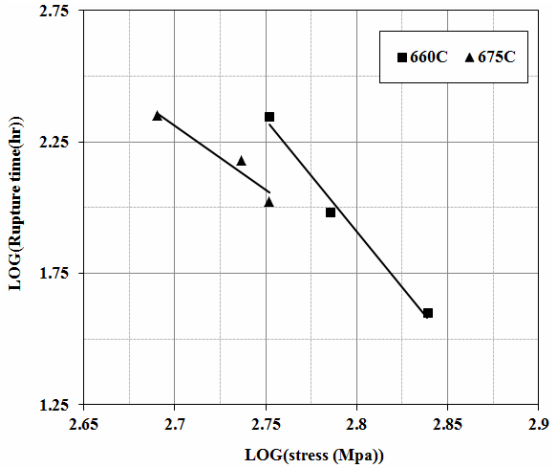

Fig. 5. Effect of the stress level on creep rupture time.

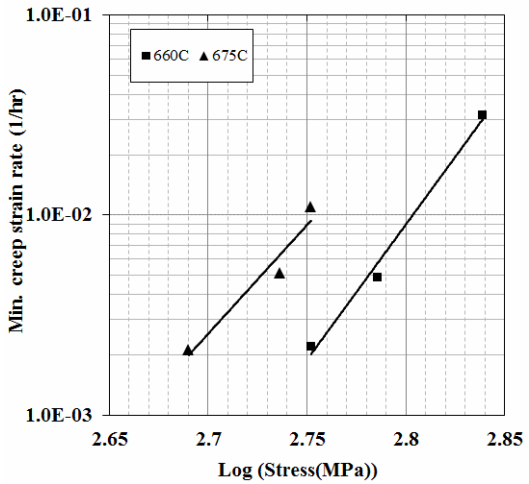

Fig. 6. Effects of the stress and temperature levels on minimum creep strain rate.

the results of the creep tests at 660 and 675°C for different stress levels are shown. The slope of the creep curves or steady state creep strain rates ($\dot{\varepsilon}_{ss}$) were obtained and given in Table 3. Fig. 5 shows the variation of the creep rupture time with stress at two temperature levels. According to Fig. 5, by increasing the stress or temperature level, time to rupture decreases significantly. The results shown in Fig. 6 also present

the logarithmic variation of minimum creep strain rate with stress level, and the linear form of the variation in logarithmic scale confirms the use of Norton-Power Law form of the constitutive equation to model the creep behavior.

3.2.1 Creep constitutive equations

The most important and widely used type of constitutive equations to predict the secondary creep is Norton-Power Law (NPL) [16]:

$$\dot{\varepsilon}_{ss} = A\sigma^n \exp(\frac{-Q}{RT}), \quad (1)$$

in which $\dot{\varepsilon}_{ss}$ is the steady state creep strain rate, σ is stress, Q is the activation energy, R is the Boltzmann gas constant, T is absolute temperature, A and n are physical constants which should be determined based on creep test data for each material. Also, to study the creep rupture time of metals, various physics-based parameters such as Larson–Miller, Monkman–Grant, Orr–Sherby–Dorn, Goldhoff–Sherby, White–Le May, have been proposed [17]. Among them, the most applicable or Larson–Miller parameter (P_{L-M}) can be expressed as:

$$P_{L-M} = T(log_{10}t_r + C)/1000 . \quad (2)$$

This equation can be derived from Eq. (1) with some simplifying assumptions. In this equation t_r is rupture time in hours and C is a physical parameter which should be determined using experimental data [18].

3.2.2 Creep properties

Creep failure is concerned in two ways: a) creep rupture time when the components actually rupture during the operation; and b) when the creep strain reaches a threshold value. To model these criteria, it is necessary to obtain creep constitutive equations. To do so, the constitutive parameters, which fit best with all test data, should be obtained using numerical optimization methods. Using these methods, the constitutive parameters can be obtained by minimizing the difference between the experimental data and the calculated values. Based on the least square summation, the total error value will be:

$$Error = \left[\sum_{i=1}^{n}\left(\dot{\varepsilon}_{\exp} - A\sigma^n \exp\left(-Q/RT\right)\right)^2\right]^{1/2}, \quad (3)$$

in which $\dot{\varepsilon}_{\exp}$ is the experimental value for the minimum creep strain rate at different stress and temperature levels. Using numerical optimization methods, the amount of "error" value was minimized and magnitudes of A, n, and Q were calculated for domestically produced IN 718 which are given in Table 4.

In Figs. 7 and 8, the experimental data and theoretical results, which are based on constitutive parameters given in Table 4, are compared.

Table 4. The parameters of constitutive equation for Inconel 718.

A ($MPa^{-n}hr^{-1}$)	Q (Kj/mol)	n
315413	767.136	12.64

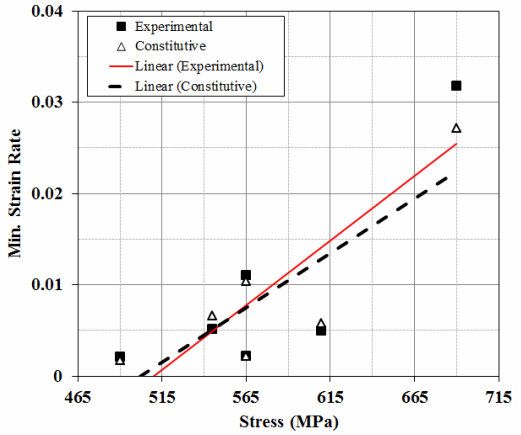

Fig. 7. Variation of the min. creep strain rate with stress and comparison of the experimental data with constitutive values.

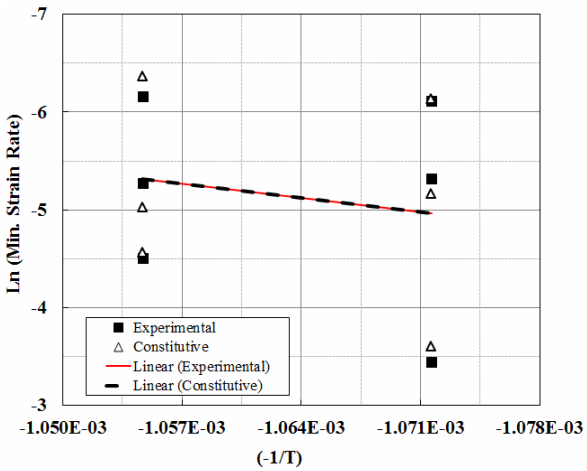

Fig. 8. Variation of the min. creep strain rate with temperature and comparison of the experimental data with constitutive values.

These figures also show that the constitutive equation can predict the experimental data with good accuracy.

In Fig. 9, the dependence of stress on the creep rupture life of IN 718 alloy is shown. By increasing stress or temperature, the creep rupture time reduces in logarithmic scale. Fig. 10 also shows the dependence of minimum creep strain rate on the applied stress.

By considering the experimental data or plotting these data on a single graph, the Larson–Miller parameter P_{L-M} can be obtained, which takes into account the mutual effects of time to failure, stress and temperature. This parameter is usually written in the form of Eq. (2). The variation of P_{L-M} was obtained using the available experimental data given in Table 3 and its variation with stress is shown in Fig. 11. In this fig-

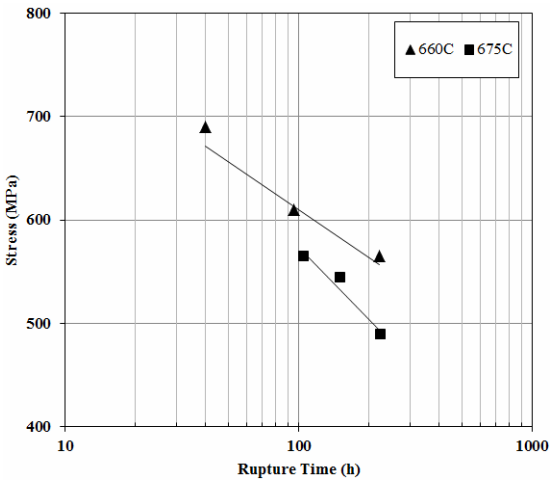

Fig. 9. The dependence of stress level on the creep rupture life.

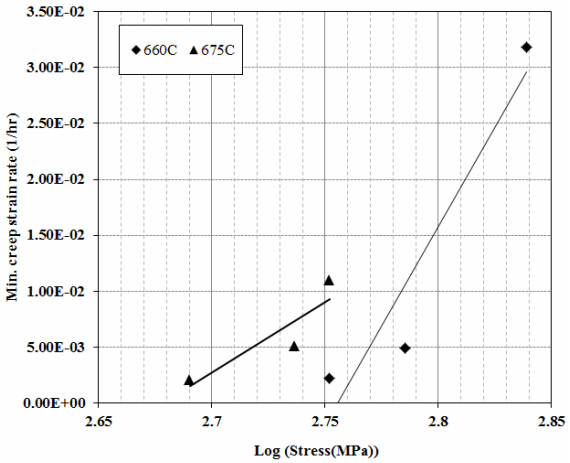

Fig. 10. The dependence of min. creep strain rate on the applied stress.

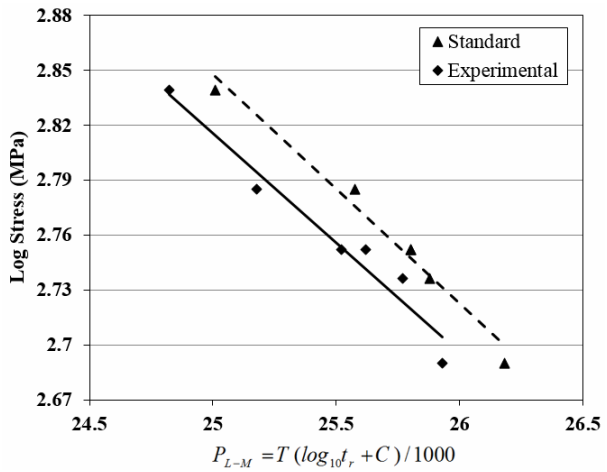

Fig. 11. P_{L-M} for tested samples and the standard values in Ref. [2].

ure, also, the values of P_{L-M} that have been obtained from the tests are compared with those that are given in standards. It is shown that the experimental data are close to the standard values. In Fig. 11, the good agreement between the results obtained in this research and those given in standards shows that the experiment-based predictions are satisfactory. Also, to validate the creep constitutive parameters which were obtained based on the experimental data (see Table 4), the creep strain-time curve produced using these parameters is compared with those proposed by Yeom and Kim et al. [1] in Fig. 12. It can be seen that the creep curves compare well with each other.

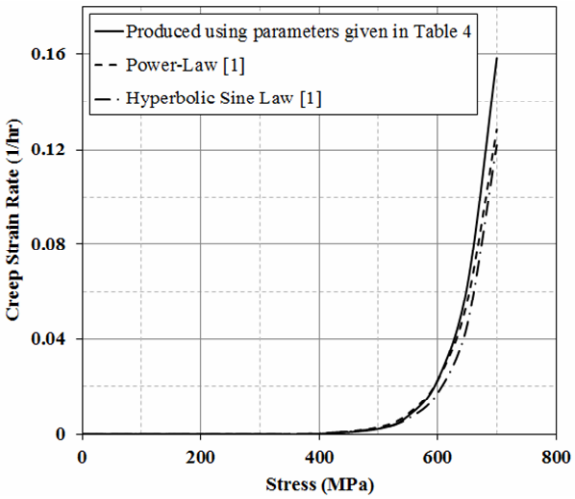

Fig. 12. Creep strain rate at 675°C obtained using parameters in Table 4 and those given by Yeom and Kim et al. [1].

To investigate the performance of the IN 718 in manufacturing gas turbine blades, their creep behavior was studied using FEM based solutions and the results were compared with those obtained for blades made of IN 738.

4. Creep behavior of gas turbine blades

Gas turbine blades are among the critical components of power plants and jet engines [19]. Therefore, creep lifetime of turbine components such as blades is becoming a major concern [20]. For example, Marahleh et al. [21] predicted the creep life of service-exposed turbine blades. Failure of gas turbine blades has also been studied by Khajavi et al. [22], Vardar et al. [23] and Mazur et al. [24]. Common failures in gas turbine blades have been studied by Carter [25].

Vaezi et al. [26] studied the creep life of IN 718 gas turbine blades via Larson-Miller parameter method. The failure analysis of a second stage blade in a gas turbine engine has been investigated by Poursaeidi et al. [27]. Chen et al. [20] studied the life prediction of turbine blades under creep–fatigue interaction. Numerical simulation of steady state heat transfer in a ceramic-coated gas turbine blade was done by Kumar at al. [28]. Furthermore, Maharaj et al. [29] modeled the creep behavior of turbine disc fir-tree made of IN 706 to optimize the operation and maintenance of the gas turbine. Based on these research works, a methodology can be developed to study the creep behavior of turbine blades. Also, different boundary,

Table 5. Chemical composition of IN 738LC (% Weight) [24].

C	Cr	Ni	Co	Mo	W
0.11	16	Bal.	8.5	1.75	2.6
Cb	Ti	Al	B	Zr	Ta
0.9	3.4	3.4	0.01	0.06	1.75

Table 6. Mechanical properties of IN 738LC at room temperature [30].

E (GPa) Young's modulus	175
ν Poisson's ratio	0.3
ρ (gr/cm^3) density	8.11
K (W/m.K) thermal conductivity	18
α (K^{-1}) thermal expansion coef.	11.6E-6
σ_y (MPa) yield strength	1000

thermal and initial conditions can be obtained which describe the range of operating condition of the gas turbines. Therefore, a set of operating conditions was obtained based on this review and used in this study.

We used the full sized modeling of a turbine blade, which includes blade body, fir-tree tenon, seal labyrinth, platform, and hoop segment. The blade is connected to a rotor with 2998 mm radius.

The model of the blade is the base of finite element analysis, which investigates the stress and strain distribution of the blade due to the thermal and mechanical loads. For this purpose, a coupled thermo-mechanical solution was carried out using finite element based computer code "Abaqus". The results of this analysis for both IN 718 and IN 738LC blades were used to estimate their creep behavior and lifetime.

4.1 Gas turbine blade properties

Chemical composition of IN 738LC is shown in Table 5 [24], and mechanical properties of this superalloy are presented in Table 6 [30].

4.1.1 Finite element modeling

The geometrical model of the blade was developed in CATIA software and imported to Abaqus software for the finite element numerical solutions (Fig. 13). To model nonlinear creep behavior accurately using finite element method, it would be more appropriate to employ nonlinear elements. On the other hand, using small sized linear elements can also predict this nonlinear behavior if the number of elements is increased and the size of elements is reduced. Usually, to model engineering components with complicated or narrow shape such as turbine blades requires using small elements with large number. Therefore, to reduce the solution time, linear elements are more favored in these cases. In this research, the blade is modeled by two types of elements, C3D8T and C3D4T. C3D8T is a linear hexahedral 8-node element and C3D4T is a linear tetrahedral 4-node element [31]. To study

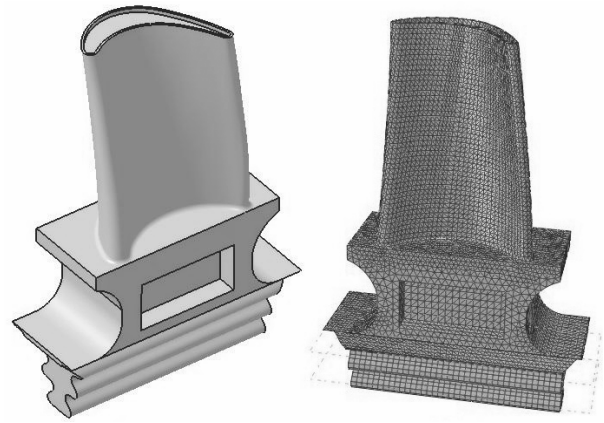

(a) (b)

Fig. 13. (a) The model of the blade in CATIA; (b) Finite element model of the blade developed in Abaqus software.

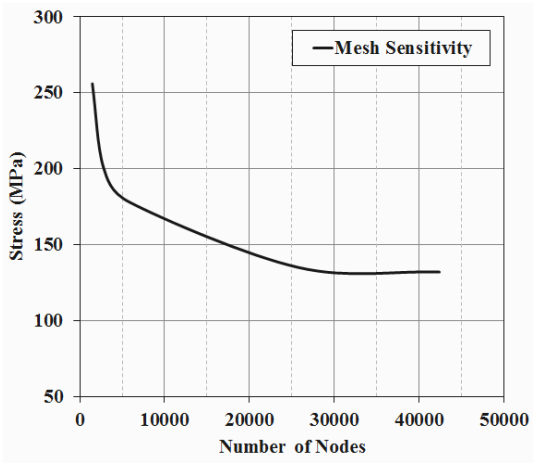

Fig. 14. Mesh sensitivity study, variation of the effective stress for an arbitrary node with the number of nodes.

the convergence of the solution and its sensitivity to the mesh and element size, a set of solutions was performed. Fig. 14 shows the effect of mesh size and number of degrees of freedom on the results of the finite element solution. This figure presents the variation of the effective stress value for the element with maximum stress, which approaches a convergence limit by increasing the number of nodes. It can be seen that to obtain accurate and converged results, a finite element mesh with 25000 nodes is required. Therefore, the total number of nodes and elements that are used in this model was set to be 25810 and 100610, respectively.

4.1.2 Boundary condition

There are different sources of loads imposed on turbine blades. Due to the rotation, the blades are subjected to centrifugal stresses ranging from 70 MPa in industrial turbine first-stage blades to 280 MPa at the airfoil root of highly cooled aircraft turbines. Superimposed on this is the stress created by the pressure difference between the positive pres-

Table 7. Boundary conditions for the turbine blade at different angular velocities [33].

Gas convection coefficient h_g(W/m^{2}K)	Gas temperature T_g(K)	Mean radius (m)	Angular velocity (rev/sec)
398	1098	0.2998	115-150

sure and suction side of the blade. The application of these stresses on the blade metal at temperature levels which often exceed 800°C results in creep [30].

For a constant section blade, the uniform centrifugal tensile stress at the root (σ_c) is given by Eq. (4) [32]

$$\sigma_c = \frac{k\rho U_t^2}{2}(1-\frac{r_h^2}{r_t^2}) \quad (4)$$

where ρ (Kg/m^3) is density, U_t (m/sec) is blade tip-speed, r_h (m) is rotor radius, r_t (m) is tip radius and k is taper factor, which is a function of the ratio of the tip to hub area [32]. The magnitude of the centrifugal stress is about ten times the bending stress [30, 32], so bending stress can be neglected.

In this research work, it is assumed that initial temperature of the blade is 552 K and fir-tree tenon remains at 552 K. The airfoil is under convection heat transfer with the properties that are shown in Table 7 at different angular velocities [33]. Thermal boundary condition of the middle part of the blade is assumed to be T_{g2} = 552(K), h_{g2} = 398(W/m^{2}K).

4.2 Prediction of the creep behavior

Various phenomenological and empirical approaches have been proposed to model the secondary creep of material [14]. For IN 738LC Hoffelner [34] has shown that the following type of constitutive equation can be used to model the creep behavior of the material:

$$\dot{\varepsilon}_c = B \cdot e^{C.\sigma_{tot}}, \quad (5)$$

where, B = 1.5E-11(sec^{-1}) and C = 2.5E-8(Pa^{-1}) are constitutive parameters at 1123 K. In this research work, the hyperbolic-sine law model:

$$\dot{\varepsilon}_{cr} = C_1(\sinh(C_2\sigma))^{C_3} \exp(\frac{-Q}{RT}) \quad (6)$$

is used to accommodate the temperature and stress dependence of this material, which is more appropriate when stress and temperature levels are high. In this equation, σ is applied stress, C_1, C_2, C_3 are material constants, Q is activation energy, R is the universal gas constant and T is temperature. To obtain material constants for IN 738LC C_1, C_2 and C_3, least square optimization scheme has been used and the values are given in Table 8.

Table 8. The value of material constants that expressed in Eq. (6).

C_1 (sec^{-1})	C_2 (MPa^{-1})	C_3
4.1095E+018	0.012462268374	2.006055295

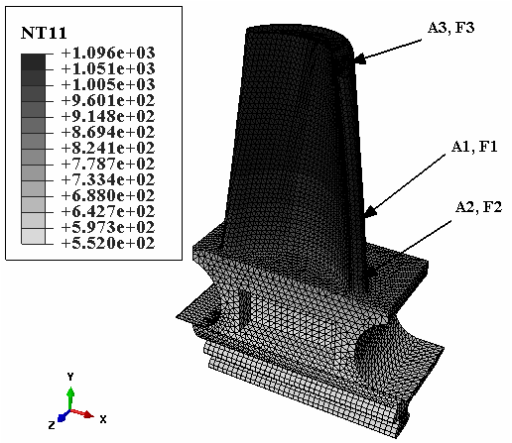

Fig. 15. Temperature contour for the blade made of IN 718.

4.2.1 Creep lifetime criterion

Creep failures of the components are categorized in two modes: creep rupture time where the components actually rupture during the operation, or when the creep strain reaches a threshold value. The latter criterion is used in almost all of the engineering components such as turbine blades. There is a gap between turbine blades and stationary casing, which is necessary to allow for the blade-rotation and mechanical or thermal deformation. This gap is known as blade-tip-gap. Since the gap between the rotor and stator is usually less than 0.001 of the rotational radius of the blade, there is a limit for creep deformation, which plays a major role in design of turbine blades [35].

4.3 Results of numerical analysis

The important locations, which have major role in designing blades, are shown in the following figures by letters (A-J) and the stress, strain and displacement of these points are presented and discussed.

4.3.1 Thermal analysis of the blade

At the first stage of each numerical solution, the temperature contours and effective thermal stresses, which are caused by the temperature gradient along the blade profile, have been obtained. Fig. 15 illustrates the temperature contour for the blade made of IN 718. It can be seen that the maximum temperature for IN 718 blade is 1096 K. The results of the numerical solutions show that the maximum temperature reaches the same value for both IN 718 and IN 738LC blades. The maximum elastic strain occurs at points A1 and F1 for IN 738LC and IN 718, respectively. In addition, the effective

Table 9. Specified points in Fig. 15 that have maximum value in thermal analysis.

	Elastic strain	Effective stress (MPa)	Displacement (mm)
IN 738LC	A1	A2	A3
	0.00653	136	0.5767
IN 718	F1	F2	F3
	0.0071	132.26	0.634

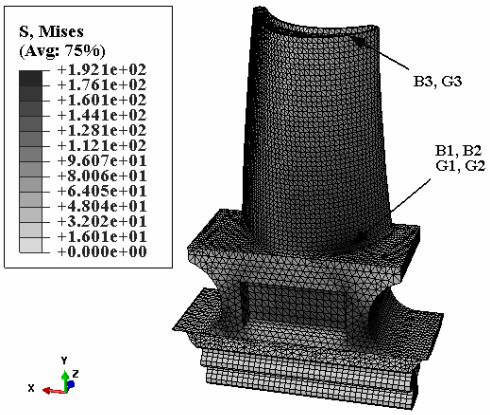

Fig. 16. Contour of the effective mechanical stress for IN 718 blade at 115 rev/sec.

stress occurs at points A2 and F2 for IN 738LC and IN 718, respectively. The maximum radial displacement caused by thermal expansion occurs at points A3 and F3.

The displacement of the tip of the blade caused by the initial heating-up should be considered in designing blade and the gap between rotor and stator, because the displacement caused by the rotational force and creep will be added to this value. Table 9 presents the maximum values of the thermal strain, stress and displacements for the blades and also identifies the locations associated with these values. Location of these points is shown in Fig. 15.

4.3.2 Mechanical solution

In this section, only the effect of mechanical loading has been obtained and thermal or creep effects have been excluded. Contours of the effective elastic stress due to the mechanical loadings for the IN 718 blade, which is operating at 115 rev/sec, are shown in Fig. 16. The maximum elastic strain occurs at points B1 and G1 for IN 738LC and IN 718, respectively. At the airfoil, maximum effective elastic stress is at the bottom of the airfoil (B2 for IN 738LC, G2 for IN 718). The maximum radial displacement occurs at points B3 and G3 for IN 738LC and IN 718 blades, respectively. The maximum values and location of these points are given in Table 10.

4.3.3 Thermomechanical solution

Contours of the initial thermomechanical effective stress and total displacement under thermal and mechanical loads

Table 10. Specified points in Fig. 16 that have maximum value at mechanical analysis.

	Elastic strain	Effective stress (MPa)	Displacement (mm)
IN 738LC	B1	B2	B3
	0.00131	213	0.0765
IN 718	G1	G2	G3
	0.00118	216.46	0.069

Table 11. Specified point in Fig. 17 that have maximum value at thermo-mechanical analysis.

	Elastic strain	Effective stress (MPa)	Displacement (mm)
IN 738LC	C1	C2	C3
	0.00663	215	0.6504
IN 718	H1	H2	H3
	0.00723	220	0.7090

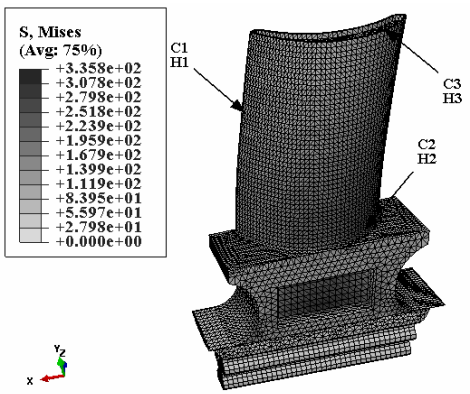

Fig. 17. Contour of the effective thermo-mechanical stress for IN 718 blade at 115 rev/sec.

have been obtained and the former is presented in Fig. 17 for IN 718 at 115 rev/sec. The maximum elastic strain occurs at points C1 and H1 for IN 738LC and IN 718 blades, respectively. The maximum effective elastic stress is at points C2 and H2. The maximum radial displacement occurs at points B3 and G3 for IN 738LC and IN 718 blades, respectively. The results for these points are shown in Table 11. Comparing the results given in Tables 10 and 11 shows that the strains are larger in thermo-mechanical solutions; also, the maximum effective stress increase from 213 MPa for mechanical solution to 215 MPa for thermomechanical solution in IN 738 blade, whereas for IN 718 it increases from 216.46 MPa to 220 MPa. This can be explained by knowing that the locations with the maximum stresses are not exactly the same in two solutions, also the direction and the values of the thermal stresses, which strongly depend on the thermal expansion of the alloys are different. The thermal expansion coefficient of IN 718 is 1.28E-5 (K^{-1}) while for IN 738 it is 1.61E-5

Table 12. Specified point in Fig. 18 that have maximum value at creep analysis after 6 and 12 years.

	Years	Creep strain	Effective stress (MPa)	Displacement (mm)
IN 738LC	6	D1	D2	D3
		5.41E-4	207.42	0.664
	12	E1	E2	E3
		8.77E-4	203.71	0.678
IN 718	6	I1	I2	I3
		8.09E-4	140.99	0.735
	12	J1	J2	J3
		9.55E-4	135.13	0.743

Table 13. Temperature level of specified points in Fig. 18.

Location	Temperature (K)
D1	1078.44
D2,E2	867.422
D3,E3,I3,J3	1096.18
E1	1078.15
I1,I2,J1,J2	868.27

(K^{-1}) [30].

4.3.4 Results of creep analysis

In Fig. 18, contours of the effective stress for the IN 718 blade operating at 115 rev/sec after 6 years are shown. Maximum creep strain occurs at points D1 and I1 for IN 738LC and IN 718, respectively. Points D2 and I2 have maximum effective stress, whereas the maximum radial displacement occurs at points D3 and I3. The values for these points are shown in Table 12.

By comparing the values of the stresses in Tables 11 and 12, it can be concluded that significant stress redistribution occurs during 6 years for IN 718. According to these tables, the value of the maximum effective stress for IN 738LC decreases from 209 to 207.42 MPa and for IN 718 it is reduced from 220 to 140.99 MPa.

Fig. 18 shows that maximum creep strain and maximum effective stress occur at different points on the airfoil for IN 738LC, whereas, for IN 718 the same location has maximum creep strain and stress. Although points D2 and E2 have higher stresses in IN 738LC blade compared to the points D1 and E1, they creep less because of their much lower temperature (see Table 13) and therefore, stress redistribution at points D2 and E2 is negligible. On the other hand, in locations D1 and E1, where creep strain is maximum, larger rate of stress redistribution or off-loading is observed due to the higher temperature level. For IN 718 blade, the points with maximum creep strain also have maximum effective stress, hence, stress redistribution occurs at a point that has maximum effective stress.

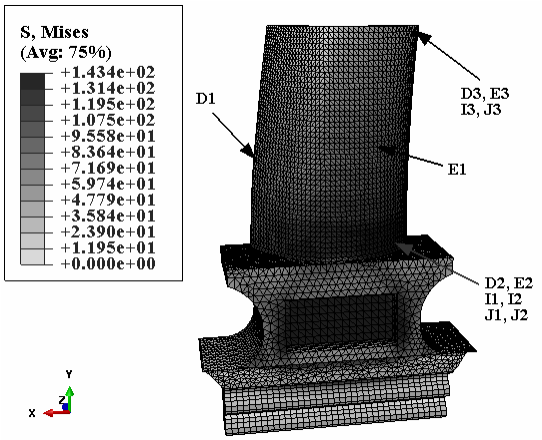

Fig. 18. Contour of the effective thermo-mechanical stress for IN 718 blade at 115 rev/sec after 6 years.

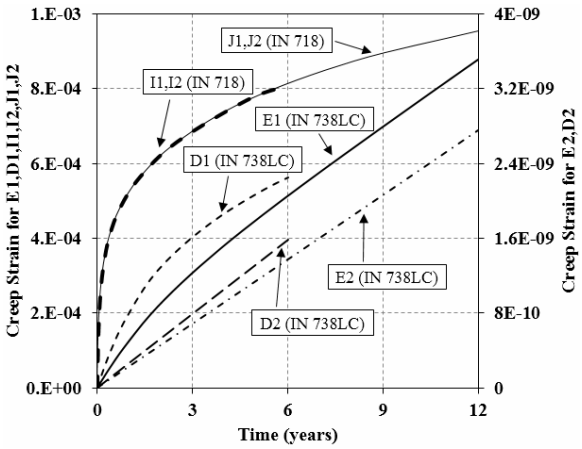

Fig. 19. Time history of creep strain during 6 and 12 years for 115 rev/sec for the blades made of IN 738LC (D,E) and IN 718(I,J).

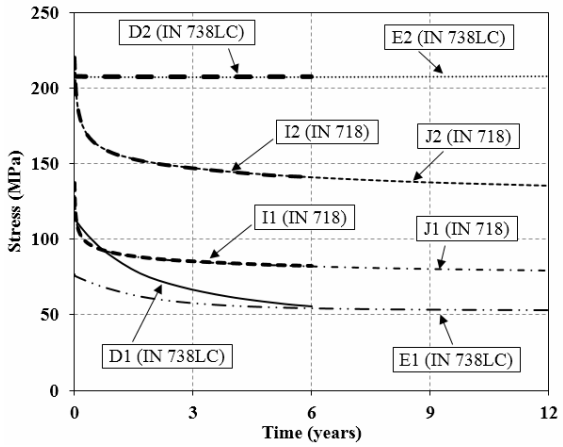

Fig. 20. Time history of stress during 6 and 12 years for 115 rev/sec for the blades made of IN 738LC (D,E) and IN 718 (I,J).

For the rotational speed of 115 rev/sec, time history of creep strain and stress is plotted in Figs. 19 and 20 during 6 and 12

Table 14. The displacement of the blade tip in mm caused by mechanical loading and creep during 6 and 12 years.

Tip displacement in mm for IN 738LC blade				
	115 (rev/sec)	130 (rev/sec)	135 (rev/sec)	150 (rev/sec)
6 years	0.0873	0.12	0.1331	0.1816
12 years	0.1012	0.1453	0.1637	0.235
Tip displacement in mm for IN 718 blade				
6 years	0.1009	0.1759	0.2271	0.739
12 years	0.1086	0.2048	0.2803	0.957

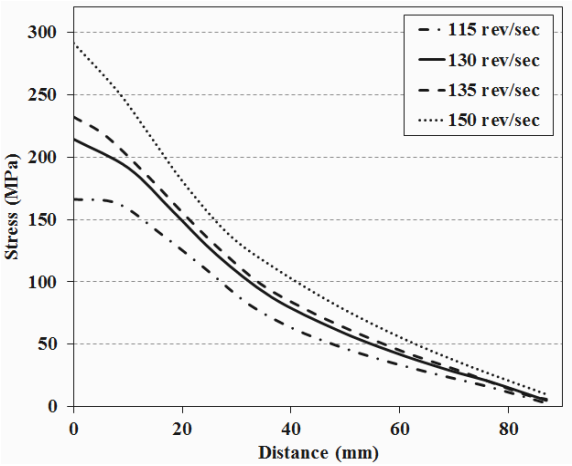

Fig. 21. Decrease of the maximum stress along the airfoil for IN738LC with different rotational speeds of the turbine.

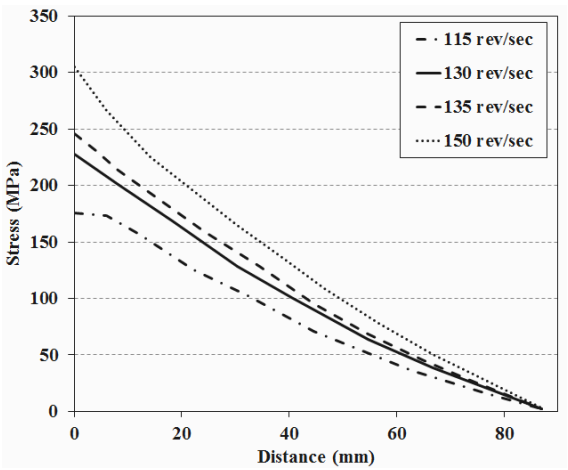

Fig. 22. Decrease of the maximum stress along the airfoil for IN 718 with different rotational speeds of the turbine.

years.

To prevent or reduce the gas leakage through the blade-tip-gap between rotor and stator, the gap-value must be less than 0.001 of its rotational radius [35]. The length of the gap for this blade is 0.2998 mm. Therefore, the working displacement or displacement due to the creep should be less than this limit. In Table 14, the displacement of the tip of the blade caused by mechanical load and creep for both blades are presented. According to this table, the tip-displacement of the IN 738LC blade is below the limit value of 0.2998 mm and this provides a safe operational condition in terms of creep behavior. However, for the blade made of IN 718, the displacement at 150 rev/sec is larger than the gap limit, whereas at lower rotational speeds (115, 130, 135 rev/sec) this blade has safe operation.

Figs. 21 and 22 show the effective stress values along the Y-axis at 115, 130, 135 and 150 rev/sec. These figures show that although the magnitude of the effective stress decreases along the length of the airfoil, stresses increase by increasing the rotational speed. This will decrease the creep lifetime of the blade significantly.

5. Conclusion

Creep behavior of the domestically produced IN 718 was investigated using experimental data. In addition, based on the test results, the creep constitutive parameters for this alloy were obtained by using numerical optimization techniques. Based on these results, the quality of the domestically produced superalloy has been verified and it has been shown that its mechanical characteristics match with the international standards. Moreover, the subject of the replacement of IN 718 with IN 738LC in producing gas turbine blades has been investigated. The results show that:

(1) The location of the maximum stress on the airfoil is at the region near the fir-tree tenon, because of the effective mass and stress concentration.

(2) The point on the airfoil with maximum stress does not produce maximum creep strain, because of its low temperature. Therefore, in terms of creep lifetime, stress concentration of the blade root loses its significance.

(3) The stress of the point that has maximum creep strain decreases more because of the off-loading due to the creep straining, so predicting the lifetime of the blade based on the effective elastic stress would be very conservative.

(4) Thermal analysis of the turbine blades is necessary not only because of the induced thermal stresses, but also due to the effect of temperature level on the creep strain. Therefore, using constant temperature solutions would lead to erroneous results.

(5) The IN 738LC blade has a safe operating life of at least 12 years in terms of creep displacement. However, the blade made of IN 718 can only be used in low and medium power gas turbines with lower rotational speed.

References

[1] J.-T. Yeom, J.-Y. Kim, Y.-S. Na and N.-K. Park, Creep strain and creep-life prediction for alloy 718 using the omega method, *Metals and Materials International*, 9 (6) (2003)

555-560.

[2] D.-H. Kim, J.-H. Kim, J.-W. Sa, Y.-S. Lee, C.-K. Park and S.-I. Moon, Stress rupture characteristics of Inconel 718 alloy for ramjet combustor, *Materials Science and Engineering A*, 483-484 (2008) 262-265.

[3] F. V. Tahami, A. H. Daei-Sorkhabi and F. R. Biglari, Creep constitutive equations for cold-drawn 304L stainless steel, *Materials Science and Engineering A*, 527 (2010) 4993-4999.

[4] Y. Han and M. C. Chaturvedi, Steady state creep deformation of superalloy inconel 718, *Materials Science and Engineering A*, 89 (1987) 25-33.

[5] A. Thomas, M. El-Wahabi, J. M. Cabrera and J. M. Prado, High temperature deformation of Inconel 718, *J. of Materials Processing Technology*, 177 (2006) 469-472.

[6] W. Chen and M. C. Chaturvedi, The effect of grain boundary precipitates on the creep behavior of Inconel 718, *Materials Science and Engineering A*, 183 (1994) 81-89.

[7] K. Ankit and N. Prasad, Simulation of creep cavity growth in Inconel 718 alloy, *Materials Science and Engineering A*, 528 (2011) 4209-4216.

[8] D. Gustafsson, *Constitutive and fatigue crack propagation behaviour of Inconel 718*, Linköpings Universitet, Electronisk Press, Linköping, Sweden (2010).

[9] J. K. Hong, J. H. Park, N. K. Park, I. S. Eom, M. B. Kim and C. Y. Kang, Microstructures and mechanical properties of Inconel 718 welds by CO_2 laser welding, *J. of Materials Processing Technology*, 201 (2008) 515-520.

[10] L. Xiao, D. L. Chen and M. C. Chaturvedi, Effect of boron on fatigue crack growth behavior in superalloy IN 718 at RT and 650°C, *Materials Science and Engineering A*, 428 (2006) 1-11.

[11] C. M. Kuo, Y. T. Yang, H. Y. Bor, C. N. Wei and C. C. Tai, Aging effects on the microstructure and creep behavior of Inconel 718 superalloy, *Materials Science and Engineering A*, 510-511 (2009) 289-94.

[12] A. Piard, D. Gamby, C. Carbou and J. Mendez, A numerical simulation of creep–fatigue crack growth in nickel-base superalloys, *Engineering Fracture Mechanics*, 71 (2004) 2299-2317.

[13] D.W. Tanner, *Life assessment of welded INCONEL 718 at high temperature*, University of Nottingham, England (2009).

[14] ASTM E8M-04 Standard test methods for tension testing of metallic materials (metric), *Annual Book of ASTM Standards*, West Conshohocken, PA, ASTM International, USA (2004).

[15] M. Urdanpilleta, J. M. Martinez-Esnaola and J. G. Sevillano, Strain rate sensitivity of superplastic Inconel 718, *Materials Transactions*, 46 (2005) 1711-1719.

[16] J. T. Boyle and J. Spence, *Stress analysis for creep*, Butterworth & Co. Ltd. (1983).

[17] J. F. dos R. Sobrinho and L. de O. Bueno, Correlation Between Creep and Hot Tensile Behaviour for 2.25 Cr-1Mo Steel from 500ºC to 700ºC. Part 2: An Assessment According to Different Parameterization Methodologies, *Revista Matéria*, 10 (2005) 463-471.

[18] F. Larson and J. Miller. A time-temperature relationship for rupture and creep stresses, *Trans ASME*, 74 (1952) 765-775.

[19] S. Barella, M. Boniardi, S. Cincera, P. Pellin, X. Degive and S. Gijbels, Failure analysis of a third stage gas turbine blade, *Engineering Failure Analysis*, 18 (2011) 386-93.

[20] L. Chen, Y. Liu and L. Xie, Power-exponent function model for low-cycle fatigue life prediction and its applications – Part I: Models and validations, *International J. of Fatigue*, 29 (2007) 1-9.

[21] G. Marahleh, A. R. I. Kheder and H. F. Hamad, Creep life prediction of service-exposed turbine blades, *Materials Science and Engineering A,* 433 (2006) 305-309.

[22] M. R. Khajavi and M. H. Shariat, Failure of first stage gas turbine blades, *Engineering Failure Analysis*, 11 (2004) 589-597.

[23] N. Vardar and A. Ekerim, Failure analysis of gas turbine blades in a thermal power plant, *Engineering Failure Analysis*, 14 (2007) 743-749.

[24] Z. Mazur, A. Luna-Ramírez, J. A. Juárez-Islas and A. Campos-Amezcua, Failure analysis of a gas turbine blade made of Inconel 738LC alloy, *Engineering Failure Analysis*, 12 (2005) 474-486.

[25] T. J. Carter, Common failures in gas turbine blades, *Engineering Failure Analysis*, 12 (2005) 237-247.

[26] M. Vaezi and M. Soleymani, Creep Life prediction of inconel 738 gas turbine blade, *J. of Applied Sciences*, 9 (2009) 1950-1955.

[27] E. Poursaeidi, M. Aieneravaie and M. R. Mohammadi, Failure analysis of a second stage blade in a gas turbine engine, *Engineering Failure Analysis*, 15 (2008) 1111-1129.

[28] N. A. Kumar and S. R. Kale, Numerical simulation of steady state heat transfer in a ceramic-coated gas turbine blade, *International J. of Heat and Mass Transfer*, 45 (2002) 4831-4845.

[29] C. Maharaj, A. Morris and J. P. Dear, Modelling of creep in Inconel 706 turbine disc fir-tree*, Materials Science and Engineering A*, 558 (2012) 412-421.

[30] A. Kountras, *Probabilistic analysis of turbine blade durability*, Massachusetts Institute of Technology, USA (2004).

[31] *ABAQUS/CAE User's Manual, Version 6.11*, Systèmes, Dassault (2012).

[32] J. Horlock, *Axial flow turbines*, *fluid mechanics and thermodynamics*, RE Krieger Publishing Company, USA (1973).

[33] M. H. Albeirutty, A. S. Alghamdi and Y. S. Najjar, Heat transfer analysis for a multistage gas turbine using different blade-cooling schemes, *Applied Thermal Engineering*, 24 (2004) 563-577.

[34] W. Hoffelner, *Creep dominated processes. High temperature alloys for gas turbines and other applications* (1986).

[35] A. Epstein et al. Micro-heat engines, GA sturbines, an d rocket engines-the met microengine project, *28th AIAA Fluid dynamics conference, 4th AIAA shear flow control conference*, Snowmass village, CO, AIAA Paper (1997) 1-12.

Farid Vakili-Tahami is currently an associate professor in Mechanical Engineering department at the University of Tabriz, Iran. He has received B.Sc. and M.Sc. in Mechanical Engineering from University of Tabriz, Iran and Ph.D. from UMIST, U.K. in 1988, 1991 and 2002, respectively. His current research interests include CDM analysis of mechanical engineering parts, creep damage of weldments, design of machine elements, numerical analysis of engineering components and FE based software coding for structural analysis.

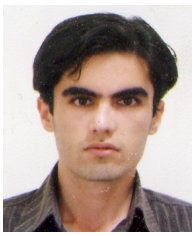

Mohammad Reza Adibeig is a Ph.D. student in Mechanical Engineering department at the University of Tabriz, Iran. He has received the B.Sc. and M.Sc. in Mechanical Engineering from University of Tabriz, Iran in 2008 and 2012, respectively. His current research interests include creep analysis of engineering parts, design of machine elements, numerical analysis of engineering components and FE based software coding for structural analysis.